Research Article | Vol. 30, No. 13 / 20 Jun 2022 / Optics Express 22860
Optics EXPRESS

High-sensitivity distributed relative salinity sensor based on frequency-scanning φ-OTDR

YUYAO WANG, HUA ZHENG,* AND CHAO LU

Research Center, Department of Electronic and Information Engineering, The Hong Kong Polytechnic University, Hong Kong, China
*hua.zheng@polyu.edu.hk

Abstract: In this paper, a high-sensitivity distributed optical fiber salinity sensor based on frequency-scanning phase-sensitive optical time-domain reflectometry (φ-OTDR) and polyimide-coated single-mode fiber is proposed. Distributed salinity sensing over an 1100 m polyimide-coated fiber with a 1 m spatial resolution was demonstrated, and a sensitivity of 782.4 MHz/(mol/L) was achieved with the salinity changing from 0 mol/L to 1.61 mol/L. Then the measurement accuracies of frequency shift and salinity were evaluated theoretically and experimentally. Both theoretical and experimental results show that the measurement accuracy deteriorates as the pulse width decreases, resulting in a trade-off between the spatial resolution and measurement accuracy. The measurement uncertainty of salinity is 0.022 mol/L in the case of 30 cm spatial resolution. And when the spatial resolution is set to be 2 m, the measurement uncertainty of salinity decreases to 0.005 mol/L. The response time of the fiber to external salinity change has also been investigated, and it takes about 8 minutes for the fiber to reach a stable state. The proposed salinity sensor exhibits high sensitivity and long measurement range, which may be used for distributed marine environmental monitoring.

1. Introduction

Salinity is an important indicator in a wide range of fields such as environmental protection, marine monitoring, agriculture production, and industrial manufacturing process control [1,2], which puts forward the demand for high performance salinity sensors. Commercially available salinity sensors generally fall into two categories, electrical and optical sensors. The electrical sensors often measure the conductivity of solutions to obtain salinity [3], and the optical methods usually use prismatic structures to measure the refractive index of the solution to indirectly obtain the salinity [4,5]. Such sensors have developed over the past several decades and have achieved high sensitivity and accuracy, but one limitation of such sensors is that they cannot be used for remote salinity measurement.

In recent years, optical fiber sensors have attracted much attention for environmental monitoring due to the advantages of corrosion resistance, safety, immunity to electromagnetic interference, and the capability of remote sensing [6–8]. So far, several types of optical fiber sensors have been reported to measure salinity, which includes fiber Bragg grating (FBG) [9,10], Sagnac interferometer [11,12], and special fiber structures [13–17]. The FBG sensors are often combined with polyimide or hydrogel coatings to achieve salinity measurement. The polyimide and hydrogel materials can absorb or lose water thereby inducing swelling or shrinkage when the external salinity changes, and the swelling and shrinkage of fiber coating will introduce radical pressure on the fiber cladding and core, thus the stress sensitive FBGs can capture the salinity of the solution surrounding the coating layer. Men *et al.* [18] proposed a salinity sensor with two cascaded FBGs, the coating layers of which were polyimide and acrylate, respectively. The proposed sensor realized simultaneous measurement of salinity and temperature with sensitivities of 0.0165 nm/(mol/L) and 0.0094 nm/°C respectively. In 2011, a more sensitive method based on Sagnac interferometer with a polyimide-coated Hi-Bi photonic crystal fiber probe was reported,

#458200 https://doi.org/10.1364/OE.458200
Journal © 2022 Received 13 Mar 2022; revised 19 Apr 2022; accepted 6 May 2022; published 8 Jun 2022

Optics EXPRESS

which claimed a sensitivity of 0.742 nm/(mol/L) [11]. The above sensors need to be fixed at the position where the salinity needs to be measured, and the salinity distribution information cannot be obtained with these kinds of sensors.

Unlike single-point optical fiber sensors, distributed optical fiber sensors (DOFS) could interrogate and spatially resolve measurands along an unmodified optical fiber. Tens of thousands single-point sensors can be effectively replaced by a DOFS comprised of a single sensing fiber, a light source, and a detector [19]. Remarkable progress has been made in the performance of DOFS over the past several decades, while the majority of research has focused on measuring the temperature, strain, and vibration. By utilizing specialty optical fibers with engineered materials or specially designed structures, DOFS could also apply to some special functionalities and applications, including gas sensing [20–22], humidity sensing [23–25], and salinity sensing. In 2020, Zhang *et al.* developed the Brillouin dynamic grating (BDG) for salinity sensing, in which a maximum sensitivity of 139.6 MHz/(mol/L) and a salinity accuracy of 0.072 mol/L were achieved in a 9 m polarization-maintaining polyimide-coated photonic crystal fiber with 15 cm spatial resolution [26]. However, the Brillouin scattering sensing mechanism makes it hard to further improve the sensitivity of the system, which limits the application of the system in high-sensitivity salinity measurement. Compared with DOFS based on Brillouin scattering, φ-OTDR based on Rayleigh scattering generally shows much higher sensitivity and is more suitable for high precision sensing. φ-OTDR can be roughly divided into two categories. Phase-resolved φ-OTDR commonly utilizes homodyne and heterodyne coherent detection to demodulate the phase change between the adjacent scattering points, which enables quantitative strain change measurement [27–30]. However, phase-resolved φ-OTDR cannot determine the algebraic sign of the strain change, which is appropriate for vibration sensing. Another category of φ-OTDR is attributed to wavelength shift demodulation, true quantitative strain change measurement including the algebraic sign can be achieved using multiple wavelength φ-OTDR, such as chirped pulse φ-OTDR [31,32] and frequency-scanning φ-OTDR [33–35]. Chirped pulse φ-OTDR employs a linearly chirped pulse to track the temperature/strain changes along sensing fiber, and does not require a frequency sweep, thus greatly decreasing the measurement time and complexity of the system [33,34]. On the other hand, frequency-scanning φ-OTDR still involves frequency sweep, which enables a higher spatial resolution. A combination of frequency-scanning φ-OTDR and BOTDA has been proposed in [35], which achieved sub-micro strain vibration measurement by the Rayleigh signal with a precision of 6.8 nε and absolute strain measurement by the Brillouin signal with 5.4 με measurement accuracy. A fast frequency-scanning φ-OTDR based pressure sensor has also been reported with a pressure coefficient of 702.5 MHz/Mpa [36]. Although various high performance φ-OTDR systems have proposed, distributed salinity sensor using φ-OTDR has not been reported yet.

In this paper, we developed the frequency-scanning φ-OTDR to achieve distributed salinity measurement, in view of the high sensitivity of Rayleigh scattering. An 1100 m single-mode fiber with 15 μm polyimide coating is used as the sensing probe, thus sensing range of 1100 m is easily reached due to the low fiber loss. Firstly, salinity ranging from 0 mol/L to 1.61 mol/L is measured with 10 ns interrogating pulse width, and the measured frequency shift shows a linear response to the salinity variation with a slope of 782.4 MHz/(mol/L). To evaluate the measurement accuracy of frequency shift of the system, experiments are carried out in case of different pulse widths, and then the measurement accuracy is discussed both theoretically and experimentally. The experimental results show that the measurement accuracy is negatively correlated with the spatial resolution of the system. As the pulse width increases from 3 ns to 20 ns, the measurement uncertainty of salinity decreases from 0.022 mol/L to about 0.005 mol/L. Then we measured the response time of the polyimide-coated fiber to salinity change, and the results show that the fiber could reach a stable state at the 8*th* minute. Finally, we made a comparison of the proposed sensor and other sensors on their performances.

Optics EXPRESS

2. Principle

The measurement principle of frequency-scanning φ-OTDR is illustrated in Fig. 1. In this scheme, the coherent optical pulse sequence with a certain frequency interval is launched into the sensing fiber, and the pulse period should be larger than the round trip time of light in fiber to avoid overlap between traces of different pulses, as shown in Fig. 1(a). The intrinsic inhomogeneities of fiber induced Rayleigh backscattering light interfere with each other within pulse width, forming jagged intensity traces, and a 3-D spectrum can be constructed by replotting the jagged intensity traces of different optical frequency pulses into one figure, as shown in the left figure of Fig. 1(b). The 3-D spectrum will remain unchanged when the sensing fiber is in a stable environment. And when a strain is applied to the sensing fiber, the phase change ($\Delta\varphi$) of Rayleigh backscattering light between position z_i and z_j will also change, which can be expressed as [37]:

$$\begin{aligned}\Delta\varphi_{ij} &= \tfrac{4\pi v}{c}(n\cdot\Delta z_{ij} + \Delta n\cdot z_{ij})\\ &= \tfrac{4\pi v}{c}(n + C_\varepsilon)\cdot z_{ij}\Delta\varepsilon\end{aligned} \tag{1}$$

where v and c are the optical frequency and velocity, Δz_{ij} and Δn represent the change of fiber length and the change of refractive index caused by strain, respectively. C_ε is the strain coefficient of refractive index and $\Delta\varepsilon$ represents the magnitude of strain applied to the fiber. This phase change can be compensated by the frequency shift (Δv) of pulses:

$$\Delta\varphi_{ij} = \frac{4\pi n z_{ij}}{c}\Delta v \tag{2}$$

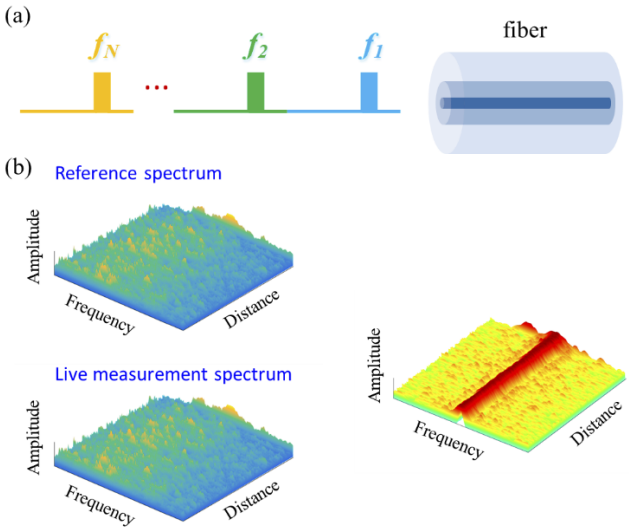

Fig. 1. (a) Principle of frequency-scanning φ-OTDR; (b) Reference and live measurement Rayleigh scattering spectra (left) and the cross-correlation spectrum between them (right).

From Eqs. (1) and (2), the relationship between the strain and the frequency shift of pulses can be derived as follows [38]:

$$\frac{\Delta v}{v} = -0.78\times\Delta\varepsilon \tag{3}$$

In the experiment, at different time stamps, we can detect the 3-D spectrum by scanning the frequency of interrogating pulses, and then the correlation spectrum can be obtained by

Optics EXPRESS

performing cross-correlation on two frequency spectra at different time stamps along the fiber distance, as shown in right figure of Fig. 1(b). At a certain position, the abscissa value of peak of correlation curve, which is referred as frequency shift in this paper, indicates the external strain change at that location. As can be seen from the cross-correlation spectrum in Fig. 1(b), there is a frequency shift at one end of fiber, indicating an external perturbation at this location.

Traditional acrylate-coated single-mode fibers are often used for temperature or strain measurements, but it is salinity insensitive. Polyimide is a hygroscopic material that swells or shrinks by absorbing or losing water when the external salinity changes. The swelling and shrinkage of polyimide coating transfer the strain on the fiber. Combining frequency-scanning φ-OTDR interrogating method and polyimide-coated sensing fiber, high-sensitivity salinity variation measurement can be achieved.

3. Experimental setup

The experimental setup of the proposed distributed salinity sensor based on frequency-scanning φ-OTDR is shown in Fig. 2. A laser with a narrow linewidth of 100 Hz and operating at a wavelength of 1550 nm is used as the light source. The frequency of the continuous light is shifted by the first electro-optic modulator (EOM1) which is operated in double-side-band (DSB) modulation mode. The frequency shift of laser is scanned by changing the output frequency of microwave generator from 8.01 GHz to 11.99 GHz with a step of 20 MHz, therefore generating 200 frequencies in total. Then the frequency shifted light is chopped into pulses through another high extinction ratio electro-optic modulator (EOM2, >40 dB) which is modulated by the output electrical pulse signal of AWG. To maximize the extinction ratio, two polarization controllers (PC) are employed at the input of each EOM. The peak power of probe pulses is amplified up to 23 dBm through an erbium-doped fiber amplifier (EDFA1) which is followed by a band-pass filter to remove the unwanted sidebands and the amplified spontaneous emission (ASE) noise. Then the probe pulses are launched into the fiber under test (FUT) with a length of 1100 m through the circulator. The Rayleigh-backscattering light from the FUT is pre-amplified by EDFA2, whose ASE noise is suppressed by another band-pass filter. A 200 MHz wide photodetector converts the optical signal into an electric voltage, which is then digitized by a fast oscilloscope with 2 GSa/s sampling rate.

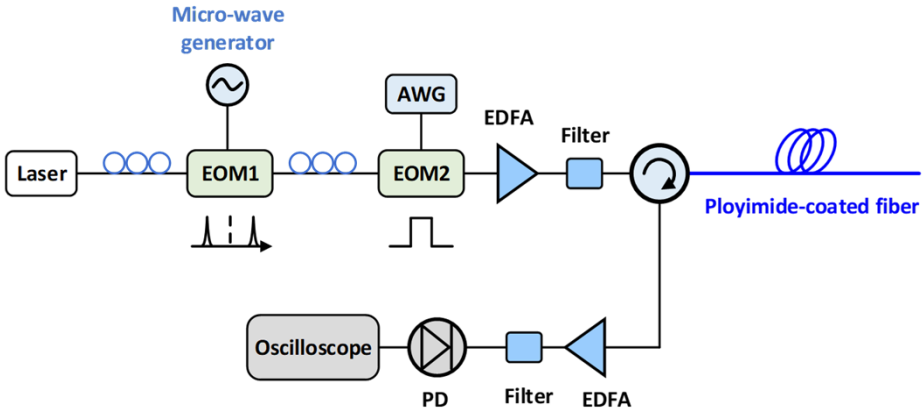

Fig. 2. Experimental setup of frequency-scanning φ-OTDR. EOM: electro-optic modulator; AWG: arbitrary waveform generator; EDFA: erbium-doped fiber amplifier; PD: photodetector.

In our experiment, the FUT is a commercially available polyimide-coated single mode fiber with a coating thickness of 15 μm. The fiber is placed in the air and the environment was relatively stable. At the far end, a section of fiber with a length of about 6 m is immersed in a water bath

Optics EXPRESS

at room temperature. Solutions with different concentrations were obtained by adding NaCl solution into pure water. For comparison, a commercially available salinometer with a nominal measurement accuracy of 0.0034 mol/L is used to measure the salinity of the solution at the same time.

4. Experimental results and discussion

4.1. Salinity measurement results

Firstly, the salinity response of the system was investigated with a pulse width of 10 ns, corresponding to a spatial resolution of 1 m. To measure the frequency shift of a certain salinity, we carried out twice 3-D Rayleigh scattering spectrum measurements, in which the fiber was immersed in pure water and NaCl solution with a certain salinity respectively. The time interval between the two measurements was set to be 10 minutes to make the fiber coating fully respond to the external salinity change. The traces were averaged 128 times to improve the SNR, thus one measurement took about 120 seconds. Fig. 3 shows the detected frequency spectra and their cross-correlation results, the salinity in this measurement was 1.33 mol/L. Figure 3(a) shows the frequency spectra at the location of 1079 m where the fiber was in the air. It is obvious that the two frequency spectra have a similar shape and do not have frequency shift, and their cross-correlation curve is shown in Fig. 3(c) in blue line. Figure 3(b) shows the frequency spectra before and after salinity change at the location of 1129 m where the fiber was immersed in the water bath. The shapes of the two spectra are also similar but there is a frequency shift between them. The cross-correlation of the two spectra is shown in Fig. 3(c) in red line. To obtain accurate frequency shift value, the peaks of cross-correlation curves were fitted using the quadratic polynomial fitting, as shown in black line in Fig. 3(c). And the corresponding abscissa value of peak of fitting curve is the frequency shift value we need. The two frequency shift values in Fig. 3(c) are 0.015 GHz and 0.893 GHz respectively.

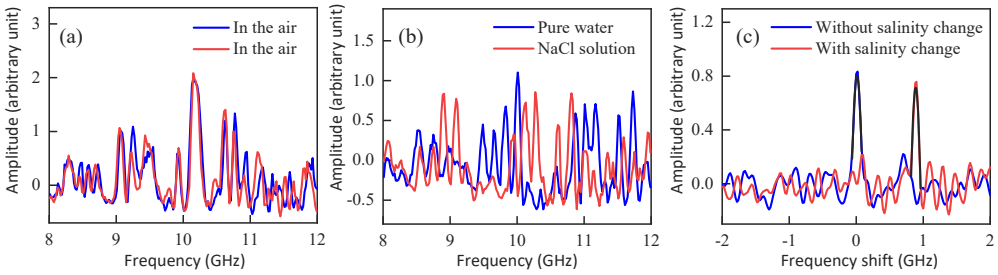

Fig. 3. The detected frequency spectra before and after salinity change at different fiber locations at the concentration of 1.33 mol/L and their cross-correlation curves. (a) The frequency spectra at the location 1079 m; (b) The frequency spectra before and after salinity change at the location 1129 m; (c) The cross-correlation curves of traces in Fig. 3(a) (blue) and Fig. 3(b) (red).

Then the cross-correlation spectrum was obtained by performing cross-correlation along the fiber distance, as shown in Fig. 4(a). It can be seen from Fig. 4(a) that the frequency shift is close to 0 when the environment remains stable. Figure 4(b) shows the enlarged spectrum as shown in the red dashed box in Fig. 4(a). A frequency shift with a length of 6 m can be observed, which matches well with the practical situation. To quantitatively describe the magnitude of frequency shift, an average over the distance between 1126.8 m and 1132.8 m is calculated, and the average value is 0.88 GHz for 1.33 mol/L salinity.

The frequency shift measurement results for different salinities are shown in Fig. 5(a). The salinity ranges from 0 mol/L to 1.61 mol/L. We can see that as the salinity increases, the frequency

Optics EXPRESS

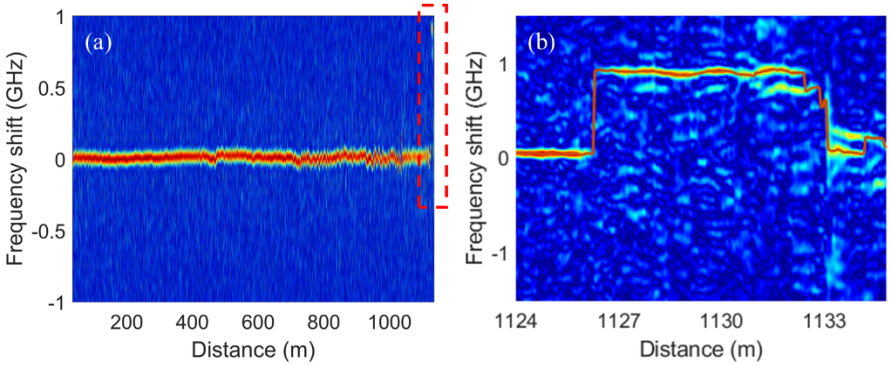

Fig. 4. (a) The cross-correlation spectrum of 3-D Rayleigh backscattering spectra in the case of pure water and 1.33 mol/L salinity solution. (b) The enlarged cross-correlation spectrum at the location near the fiber end.

shift increases accordingly. The average frequency shift in Fig. 5(a) is plotted as a function of salinity, as shown in Fig. 5(b). The frequency shift has a linear relationship with salinity. And the fitting curve of the experimental results has a slope of 782.4 MHz/(mol/L) and a coefficient of determination of 0.9595, suggesting a high salinity sensitivity of the system. It is worth noting that the dynamic range of the system is not restricted to 1.61 mol/L, since it can be easily increased by enlarging the frequency sweep range of probe pulses.

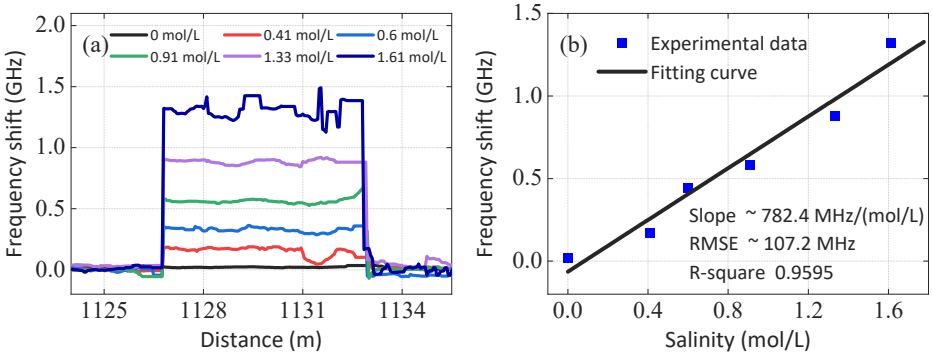

Fig. 5. (a) The measured frequency shift of different salinities; (b) the frequency shift variation with salinity.

As can be seen from Fig. 5(a), the frequency shift fluctuates over the distance between 1126.8 m and 1132.8 m, especially in the case of salinity of 0.41 mol/L and 1.61 mol/L. The uniformity of the frequency shift can be affected by different reasons such as the uniformity of NaCl solution, the contact between the fiber and solution, and the environmental perturbations. Since each salinity was measured independently, these experimental conditions might be slightly different in different measurements. The dip at 1131.5 m at the salinity of 0.41 mol/L might result from the insufficient contact between the fiber and the solution, and the fluctuation in the case of 1.61 mol/L salinity might be a comprehensive result of the nonuniformity of NaCl solution and the environmental perturbations.

Optics EXPRESS

4.2. Evaluation of salinity measurement accuracy

In our experiment, for each salinity, the 3-D Rayleigh scattering spectra were measured once in pure water and once in saline solution, and the cross-correlation of the two spectra provided the measured frequency shift results. The measurement accuracy of frequency shift provided by cross-correlation can be affected by various factors such as pulse shape, pulse width, and signal noise ratio (SNR) of Rayleigh backscattering trace [39].

In this study, we experimentally investigated the measurement accuracy of frequency shift and compared it with the theoretical value. To investigate the measurement accuracy of frequency shift in the case of different pulse widths, a group of measurements were carried out. The pulse widths in this group of measurements were set to be 20 ns, 10 ns, 5 ns, and 3 ns respectively, the salinities were 1.33 mol/L in four experiments, and other parameters were the same as those in section 3. The measured cross-correlation spectra in the case of different pulse widths are shown in Fig. 6, and the red lines in the figures represent the frequency shift along the fiber length.

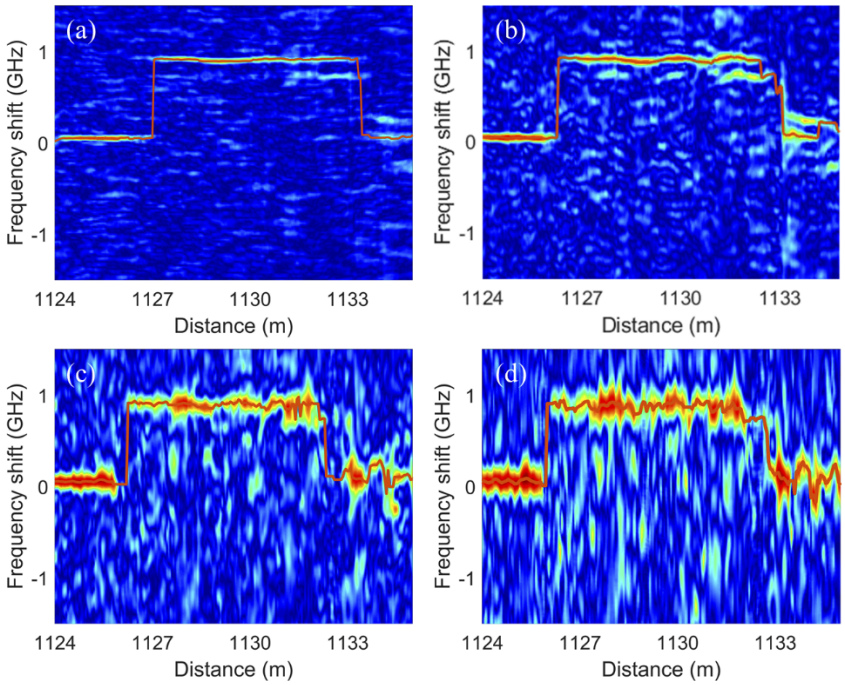

Fig. 6. The measured cross-correlation spectra near the fiber end with pulse widths of (a) 20 ns; (b) 10 ns; (c) 5 ns; (d) 3 ns.

It is obvious in Fig. 6 that as the pulse width decreases, the fluctuation of the frequency shift gets larger. Since the measurement results of frequency shift at different fiber locations are independent, the frequency shift measurement uncertainties can be characterized by the standard deviation of frequency shift at different fiber locations. From Fig. 4(a) we can see that the frequency uncertainties at different positions are different. The fluctuation at the position of 800 m is larger than that at the position of 200 m, which results from random ambient perturbations like temperature change. Since the environmental perturbation is random and different at different fiber locations, we calculate the standard deviation every 2.5 m and an average of standard deviations was calculated from 0 m to 960 m. The results for different pulse widths are plotted in Fig. 7 in magenta dots. The vertical axis on the left shows the frequency shift measurement uncertainty and the vertical axis on the right shows the corresponding salinity measurement

Optics EXPRESS

uncertainty with a coefficient of 782.4 MHz/(mol/L). The theoretical curve in black solid line is determined by the equation [39]:

$$\sigma = \frac{\sqrt{6}}{2\pi\tau M} \tag{4}$$

where τ and M represent pulse width and SNR of the Rayleigh backscattering signal, respectively. In Fig. 7, the measured frequency uncertainties are larger than the theoretical frequency uncertainties. This is reasonable because the ambient perturbation will also result in measurement error although an average was used. Since the spatial resolution of the system is determined by the interrogating pulse width launched into sensing fiber, a trade-off between the spatial resolution and salinity measurement accuracy is required. The salinity uncertainty in the case of 20 ns is 0.005 mol/L (corresponding to 3.7 MHz frequency uncertainty), while the salinity uncertainty in the case of 3 ns is 0.022 mol/L (corresponding to 17.6 MHz frequency uncertainty). The experimental results prove the high accuracy and reliability of this method.

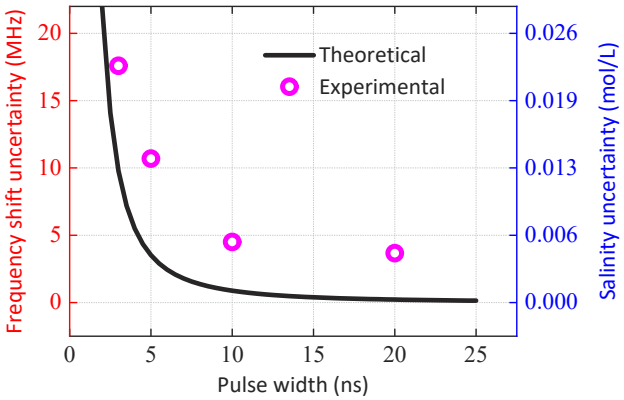

Fig. 7. The measurement accuracy of frequency shift and salinity in case of different pulse widths.

4.3. Response time

Then we tested the response time of the fiber to salinity change. In this experiment, the frequency shift of optical pulses was swept from 9.765 GHz to 14.235 GHz at a step of 30 MHz, thus generating 150 frequencies in total. To make each measurement faster, the average time of traces was set to be 64, and the time taken for each Rayleigh backscattering spectrum measurement was 44.2 seconds. The response times of salinity 0.48 mol/L and 1.76 mol/L were measured with 3 ns pulse width respectively. For each salinity, we collected 18 Rayleigh spectra consecutively starting from the NaCl solution added into pure water, which took 13.3 minutes in total. Then the cross-correlation was performed to the adjacent spectra and 17 frequency shift curves were obtained. The results for different salinities are shown in Fig. 8. As time goes by, the magnitude of frequency shift decreases, and the fiber reaches a stable state gradually. The frequency shift almost reaches zero at the time of 8 min.

4.4. Comparison with other fiber-optic sensors

Table 1 compares the salinity measurement performances of our salinity sensor with previous fiber-optic sensors. The proposed sensor employs an unmodified polyimide-coated single-mode fiber as a sensing medium, distributed salinity sensing can be realized over long distance and no complex process is required. Meanwhile, the proposed sensor shows a high salinity sensitivity, which enables a good measurement accuracy. However, the sensor is also sensitive to temperature

Optics EXPRESS

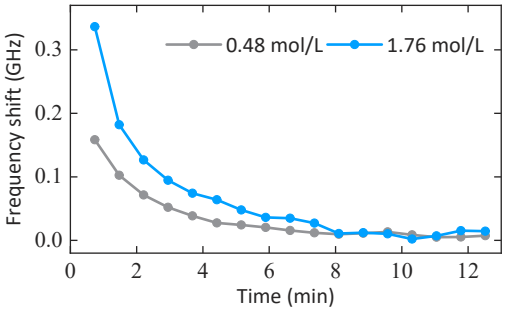

Fig. 8. The response time of the fiber to salinity change

variation, which limits its long-term stability. Subsequent research may include how to eliminate crosstalk between salinity and temperature.

Table 1. Comparison of our method with other fiber-optic sensors

Technique	Sensitivity	Spatial resolution	Sensing range	Ref
FBG	15.40 nm/RI	N.A.	N.A.	[40]
MZI	64 pm/‰	N.A.	N.A.	[41]
FPI	0.45 nm/(mol/L)	N.A.	N.A.	[16]
SPR	0.3769 nm/‰	N.A.	N.A.	[42]
BDG	119 MHz/(mol/L)	15 cm	9 m	[26]
This work	782 MHz/(mol/L)	30 cm	1 km	

5. Conclusion

In summary, we proposed a distributed high-sensitivity salinity sensor which combines frequency-scanning φ-OTDR and polyimide-coated fiber in this paper. The hygroscopic property of polyimide makes the fiber coating swell or shrink when the environmental salinity changes, thereby realizing salinity measurement. In our experiment, a salinity sensitivity of 782.4 MHz/(mol/L) was achieved on an 1100 m fiber with 15 µm polyimide coating. The measurement accuracy of frequency-scanning φ-OTDR was also investigated theoretically and experimentally. And the investigation results show that there is a trade-off between the spatial resolution and measurement accuracies of frequency shift and salinity. According to the experimental results, the measurement uncertainties of salinity are 0.005 mol/L and 0.022 mol/L in the case of 20 ns and 3 ns interrogating pulse widths respectively. We also measured the response time of the fiber to the salinity change, which was both 8 minutes in the case of 0.48 mol/L and 1.76 mol/L salinity changes. Finally, we compared our method with other fiber-optic sensors, our method can achieve remote sensing of salinity with high sensitivity and large sensing range, which makes it a promising candidate for salinity measurement in practical applications in the future.

Funding. Research Grant Council of the Hong Kong SAR Government (PolyU, 15209919).

Disclosures. The authors declare no conflicts of interest

Data availability. Data underlying the results presented in this paper are not publicly available at this time but may be obtained from the authors upon reasonable request.

References

1. F. Adamo, F. Attivissimo, C. G. C. Carducci, and A. M. L. Lanzolla, "A smart sensor network for sea water quality monitoring," IEEE Sensors J. **15**(5), 2514–2522 (2015).

Optics EXPRESS

2. S. Hosoda, T. Suga, N. Shikama, and K. Mizuno, "Global surface layer salinity change detected by Argo and its implication for hydrological cycle intensification," J. Oceanogr. **65**(4), 579–586 (2009).
3. R. A. Cox, F. Culkin, and J. Riley, "The electrical conductivity/chlorinity relationship in natural sea water," in *Deep Sea Research and Oceanographic Abstracts* (Elsevier, 1967), 14(2), pp. 203–220.
4. A. W. Domanski, M. Roszko, and M. Swillo, "Compact optical fiber refractive index differential sensor for salinity measurements," in IEEE Instrumentation and Measurement Technology Conference Sensing, Processing, Networking. IMTC Proceedings (IEEE, 1997), 2, pp. 953–956.
5. H. Minato, Y. Kakui, A. Nishimoto, and M. Nanjo, "Remote refractive index difference meter for salinity sensor," IEEE Trans. Instrum. Meas. **38**(2), 608–612 (1989).
6. A. Barrias, J. R. Casas, and S. Villalba, "A review of distributed optical fiber sensors for civil engineering applications," Sensors **16**(5), 748 (2016).
7. J.-M. Henault, G. Moreau, S. Blairon, J. Salin, J.-R. Courivaud, F. Taillade, E. Merliot, J.-P. Dubois, J. Bertrand, S. Buschaert, and and others, "Truly distributed optical fiber sensors for structural health monitoring: From the telecommunication optical fiber drawling tower to water leakage detection in dikes and concrete structure strain monitoring," Advances in Civil Engineering **2010**, 1–13 (2010).
8. A. Barrias, G. Rodriguez, J. R. Casas, and S. Villalba, "Application of distributed optical fiber sensors for the health monitoring of two real structures in Barcelona," Structure and Infrastructure Engineering **14**(7), 967–985 (2018).
9. J. Cong, X. Zhang, K. Chen, and J. Xu, "Fiber optic Bragg grating sensor based on hydrogels for measuring salinity," Sens. Actuators, B **87**(3), 487–490 (2002).
10. D. A. Pereira, O. Frazao, and J. L. Santos, "Fiber Bragg grating sensing system for simultaneous measurement of salinity and temperature," Opt. Eng **43**(2), 299–304 (2004).
11. C. Wu, B.-O. Guan, C. Lu, and H.-Y. Tam, "Salinity sensor based on polyimide-coated photonic crystal fiber," Opt. Express **19**(21), 20003–20008 (2011).
12. C. Wu, L. Sun, J. Li, and B.-O. Guan, "Highly sensitive evanescent-wave water salinity sensor realized with rectangular optical microfiber Sagnac interferometer," in *23rd International Conference on Optical Fibre Sensors* (International Society for Optics and Photonics, 2014), 9157, p. 915758.
13. D. Vigneswaran, N. Ayyanar, M. Sharma, M. Sumathi, M. Rajan, and K. Porsezian, "Salinity sensor using photonic crystal fiber," Sens. Actuators, A **269**, 22–28 (2018).
14. M. Jaddoa, A. A. Jasim, M. Razak, S. W. Harun, and H. Ahmad, "Highly responsive NaCl detector based on inline microfiber Mach–Zehnder interferometer," Sens. Actuators, A **237**, 56–61 (2016).
15. Q. Meng, X. Dong, K. Ni, Y. Li, B. Xu, and Z. Chen, "Optical fiber laser salinity sensor based on multimode interference effect," IEEE Sensors J. **14**(6), 1813–1816 (2014).
16. X. Zhang and W. Peng, "Temperature-independent fiber salinity sensor based on Fabry-Perot interference," Opt. Express **23**(8), 10353–10358 (2015).
17. D. Z. Stupar, J. S. Bajić, A. V. Joža, B. M. Dakić, M. P. Slankamenac, M. B. Živanov, and E. Cibula, "Remote monitoring of water salinity by using side-polished fiber-optic U-shaped sensor," in *2012 15th International Power Electronics and Motion Control Conference (EPE/PEMC)* (IEEE, 2012), pp. LS4c-4.
18. L. Men, P. Lu, and Q. Chen, "A multiplexed fiber Bragg grating sensor for simultaneous salinity and temperature measurement," J. Appl. Phys. (Melville, NY, U. S.) **103**(5), 053107 (2008).
19. H. Zheng, J. Zhang, N. Guo, and T. Zhu, "Distributed Optical Fiber Sensor for Dynamic Measurement," J. Lightwave Technol. **39**(12), 3801–3811 (2021).
20. A. Garcia-Ruiz, J. Pastor-Graells, H. F. Martins, K. H. Tow, L. Thévenaz, S. Martin-Lopez, and M. Gonzalez-Herraez, "Distributed photothermal spectroscopy in microstructured optical fibers: towards high-resolution mapping of gas presence over long distances," Opt. Express **25**(3), 1789–1805 (2017).
21. Y. Lin, F. Liu, X. He, W. Jin, M. Zhang, F. Yang, H. L. Ho, Y. Tan, and L. Gu, "Distributed gas sensing with optical fibre photothermal interferometry," Opt. Express **25**(25), 31568–31585 (2017).
22. M. R Fernández-Ruiz, L. Costa, and H. F Martins, "Distributed acoustic sensing using chirped-pulse phase-sensitive OTDR technology," Sensors **19**(20), 4368 (2019).
23. S. Liehr, M. Breithaupt, and K. Krebber, "Distributed humidity sensing in PMMA optical fibers at 500 nm and 650 nm wavelengths," Sensors **17**(4), 738 (2017).
24. P. J. Thomas and J. O. Hellevang, "A high response polyimide fiber optic sensor for distributed humidity measurements," Sens. Actuators, B **270**, 417–423 (2018).
25. T. F. Neves, L. Zhang, F. Yang, K. H. Tow, P. Petagna, and L. Thévenaz, "A kilometre-range distributed relative humidity sensor," in *Seventh European Workshop on Optical Fibre Sensors* (International Society for Optics and Photonics, 2019), 11199, p. 1119922.
26. H. Zhang, L. Teng, and Y. Dong, "Distributed Salinity Sensor With a Polyimide-Coated Photonic Crystal Fiber Based on Brillouin Dynamic Grating," J. Lightwave Technol. **38**(18), 5219–5224 (2020).
27. Z. Wang, L. Zhang, S. Wang, N. Xue, F. Peng, M. Fan, W. Sun, X. Qian, J. Rao, and Y. Rao, "Coherent Φ-OTDR based on I/Q demodulation and homodyne detection," Opt. Express **24**(2), 853–858 (2016).
28. G. Yang, X. Fan, S. Wang, B. Wang, Q. Liu, and Z. He, "Long-range distributed vibration sensing based on phase extraction from phase-sensitive OTDR," IEEE Photonics J. **8**(3), 1–12 (2016).
29. D. Chen, Q. Liu, Y. Wang, H. Li, and Z. He, "Fiber-optic distributed acoustic sensor based on a chirped pulse and a non-matched filter," Opt. Express **27**(20), 29415–29424 (2019).

Optics EXPRESS

30. J. Zhang, H. Wu, H. Zheng, J. Huang, G. Yin, T. Zhu, F. Qiu, X. Huang, D. Qu, and Y. Bai, "80 km fading free phase-sensitive reflectometry based on multi-carrier NLFM pulse without distributed amplification," J. Lightwave Technol. **37**(18), 4748–4754 (2019).
31. L. Marcon, M. A. Soto, M. Soriano-Amat, L. Costa, H. F. Martins, L. Palmieri, and M. Gonzalez-Herraez, "Boosting the spatial resolution in chirped pulse φ-OTDR using sub-band processing," in *Seventh European Workshop on Optical Fibre Sensors* (International Society for Optics and Photonics, 2019), 11199, p. 111991W.
32. R. Magalhaes, T. F. P. D. Neves, L. Scherino, S. Martin-Lopez, and H. F. Martins, "Reaching long-term stability in CP-OTDR," Journal of Lightwave Technology (2022).
33. J. Pastor-Graells, H. F. Martins, A. Garcia-Ruiz, S. Martin-Lopez, and M. Gonzalez-Herraez, "Single-shot distributed temperature and strain tracking using direct detection phase-sensitive OTDR with chirped pulses," Opt. Express **24**(12), 13121–13133 (2016).
34. M. R. Fernández-Ruiz, J. Pastor-Graells, H. F. Martins, A. Garcia-Ruiz, S. Martin-Lopez, and M. Gonzalez-Herraez, "Laser phase-noise cancellation in chirped-pulse distributed acoustic sensors," J. Lightwave Technol. **36**(4), 979–985 (2018).
35. B. Wang, D. Ba, Q. Chu, L. Qiu, D. Zhou, and Y. Dong, "High-sensitivity distributed dynamic strain sensing by combining Rayleigh and Brillouin scattering," Opto-Electron. Adv. **3**(12), 20001301 (2020).
36. L. Qiu, D. Ba, D. Zhou, Q. Chu, Z. Zhu, and Y. Dong, "High-sensitivity dynamic distributed pressure sensing with frequency-scanning φ-OTDR," Opt. Lett. **47**(4), 965–968 (2022).
37. Y. Dong, X. Chen, E. Liu, C. Fu, H. Zhang, and Z. Lu, "Quantitative measurement of dynamic nanostrain based on a phase-sensitive optical time domain reflectometer," Appl. Opt. **55**(28), 7810–7815 (2016).
38. Y. Koyamada, M. Imahama, K. Kubota, and K. Hogari, "Fiber-optic distributed strain and temperature sensing with very high measurand resolution over long range using coherent OTDR," J. Lightwave Technol. **27**(9), 1142–1146 (2009).
39. M. Galal, S. Sebastian, Z. Yang, L. Zhang, S. Zaslawski, and L. Thévenaz, "On the measurement accuracy of coherent Rayleigh-based distributed sensors," Opt. Express **29**(26), 42538–42552 (2021).
40. D. Luo, J. Ma, Z. Ibrahim, and Z. Ismail, "Etched FBG coated with polyimide for simultaneous detection the salinity and temperature," Opt. Commun. **392**, 218–222 (2017).
41. S. Wang, T. Liu, X. Wang, Y. Liao, J. Wang, and J. Wen, "Hybrid structure Mach-Zehnder interferometer based on silica and fluorinated polyimide microfibers for temperature or salinity sensing in seawater," Measurement **135**, 527–536 (2019).
42. E. Siyu, Y.-N. Zhang, B. Han, W. Zheng, Q.-L. Wu, and H.-K. Zheng, "Two-channel surface plasmon resonance sensor for simultaneous measurement of seawater salinity and temperature," IEEE Trans. Instrum. Meas. **69**(9), 7191–7199 (2020).